IEEE Access
Multidisciplinary | Rapid Review | Open Access Journal

Received August 24, 2021, accepted September 13, 2021, date of publication September 20, 2021, date of current version September 29, 2021.

Digital Object Identifier 10.1109/ACCESS.2021.3114100

Saturated Visual-Servoing Control Strategy for Nonholonomic Mobile Robots With Experimental Evaluations

RICARDO PÉREZ-ALCOCER[1], LUIS GONZALO MONTOYA-VILLEGAS[2], ANGEL EDUARDO LOPEZ-MARTINEZ[2], AND JAVIER MORENO-VALENZUELA[2], (Member, IEEE)
[1]CONACYT-Instituto Politécnico Nacional-CITEDI, Tijuana, Baja California 22435, Mexico
[2]Instituto Politécnico Nacional, CITEDI, Tijuana, Baja California 22435, Mexico

Corresponding author: Luis Gonzalo Montoya-Villegas (lmontoya@citedi.mx)

This work was supported in part by the Secretaría de Investigación y Posgrado del Instituto Politécnico Nacional under Research Grant 20210792, in part by CONACYT Project Cátedras under Grant 1537, and in part by the Consejo Nacional de Ciencia y Tecnología (Proyecto Apoyado por el Fondo Sectorial de Investigación para la Educación) under Project A1-S-24762, Mexico.

ABSTRACT A novel saturated visual control strategy for nonholonomic mobile robots is presented. The principal focus is to deal with the stabilization problem. The saturation bounds for the control actions avoid exceeding the physical restrictions of the actuators. This feature is the main difference concerning related works. The closed-loop system is analyzed using the theory of non-autonomous cascade systems, and global uniform asymptotic stability is guaranteed. Experimental validation is carried out by using a unicycle-type mobile robot with an onboard camera. The experiment consists of stabilizing the robot in a preset pose using visual information. The experimental results are compared with a literature unsaturated visual servoing strategy. The results confirm the effectiveness of the proposed approach, completing the assigned task and bounding the control inputs.

INDEX TERMS Mobile robot, real-time experiments, saturated control, stabilization problem, visual servoing.

I. INTRODUCTION

Visual servoing is a common technique nowadays. This control technique allows controlling the movements of the robots by using image information. Usually, onboard cameras are the most popular to obtain information due to the autonomy that brings to the robotic system. Some recently reported works have applied this technique to different robot types. In [1], a robust uncalibrated visual servoing methodology based on disturbance observer was tested in a NAO robot. Xie and Lynch [2] presented a state transformation-based dynamic visual servoing scheme for a quadrotor. A Finite-time-based PD+ control scheme for uncalibrated robot manipulator based on visual servoing was designed in [3]. The authors of [4] proposed a hybrid visual servo controller for underwater vehicles. The results of [5] showed a review study that discusses the design of an arm-robot manipulator applied in agriculture by position-based visual servoing and edge detection for image processing. Zheng *et al.* [6] introduced a method to preserve visibility during the visual servoing of quadrotors. In [7], an image-based dynamic visual servoing scheme for an octopus tentacle-like soft robot arm working in an underwater environment was designed. An adaptive neuronal networks-based visual control for a manipulator with visibility constraint and unknown dead-zone input was developed in [8]. The authors of [9] addressed the robust position-based visual control problem for a quadrotor with a down-facing monocular camera to perform ground target tracking tasks in outdoor environments. The results of [10] showed the performance of an image-based visual controller applied to the six degrees of freedom robot.

Specifically, visual servoing for mobile robots is a practical solution for vehicle navigation. This technique is useful to perform tasks that require the perception of the external environment, including stabilization and tracking problems. The most popular camera configuration is the camera mounted

The associate editor coordinating the review of this manuscript and approving it for publication was Min Wang.

in the mobile robot in order to keep the object of interest in the field view. Recent works that address visual control for mobile robots are described following. In [11], a controller for visual servoing trajectory tracking of nonholonomic mobile robots without direct position measured was presented. An image-based visual servoing controller for mobile robots was proposed in [12] by using the radial camera model. Zhang *et al.* [13] designed a visual servoing strategy for nonholonomic mobile robots despite unknown extrinsic camera-to-robot parameters. The authors of [14] provided a model-free visual servoing strategy to drive a wheeled mobile robot to the desired pose without the desired image. Qiu *et al.* [15] developed a concurrent learning-based visual servo tracking scheme with scene depth identification for wheeled mobile robots. A visual servo tracking scheme for wheeled mobile robots under the presence of uncalibrated translational camera-to-robot parameters was proposed in [16]. The results of [17] shown a mobile robot visual servoing based global path planning method based on interval type-2 fuzzy logic using an overhead camera. In [18], two uncalibrated visual control schemes for wheeled mobile robots with uncertain model parameters in complex environments were developed.

In particular, the stabilization problem for nonholonomic mobile robots using visual feedback is one of the most interesting current topics. Hence, there are many works in this field. For example, in [19], an adaptive visual servoing strategy was proposed to regulate the mobile robot to the desired pose. Lu *et al.* [20] presented a global adaptive controller for tracking and regulation problems simultaneously applied to wheeled mobile robots with depth and uncalibrated camera-to-robot extrinsic parameters. An image-based position control scheme for nonholonomic mobile robots without knowing the camera parameters was designed in [21]. The authors of [22] constructed a visual servoing strategy to steer a wheeled mobile robot to the desired pose, in which unknown depth information is simultaneously identified. Sharma *et al.* [23] developed a position-based visual servoing scheme able to estimate body-to-camera parameters online. The results in [24] showed an optimization stabilization method for visual servo control of nonholonomic mobile robots with fixed monocular cameras onboard. In [25], an approach to the uncalibrated visual stabilization of nonholonomic mobile robots was given. Finally, an adaptive two-stage switching approach to stabilize the visual servoing system in the presence of both uncalibrated camera-to-robot parameters and unknown image depth was proposed in [26].

Nevertheless, all the aforementioned studies were designed without considering the saturation phenomenon presented in the actuators of nonholonomic mobile robots. To include this feature in the design is essential to avoid unreachable control actions. Besides, saturated inputs applied to nonholonomic vehicles limit the movement velocities and prevent the feature point go away from the camera's field of view in visual servoing schemes. Controllers that deliver saturated inputs have recently been proposed. However, these works lack visual feedback. For example, in [27], a finite-time sliding-mode controller with input voltage saturation for an omnidirectional mobile robot was designed. Huang *et al.* [28] presented a robust network-based control scheme for tracking and stabilization problems simultaneously applied to a wheeled mobile robot subject to parametric uncertainties, external disturbances, and input torque saturation. In [29], an extended state observer-based adaptive sliding mode tracking controller for wheeled mobile robots with input voltage saturation and uncertainties was presented. The global consensus problem for nonholonomic mobile robots was solved by using distributed velocity saturated controllers in [30]. In [31], a family of velocity saturated controllers for unicycle-type wheeled mobile robots was proposed. Li and Wang [32] addressed the consensus control problem for wheeled mobile robots under linear speed saturation.

In an exhaustive literature review, only two papers were found addressing the stabilization problem of a unicycle-type wheeled mobile robot using a saturated visual controller [33], [34]. The closed-loop stability analysis reported in [33] is supported by LaSalle's invariance principle. However, the closed-loop system is non-autonomous, so this theorem cannot be applied. Besides, the authors did not present any experimental evidence. Therefore, the saturated visual servoing scheme is an important and not well-studied research topic. In this paper, a saturated visual controller is presented in order to improve the existing solutions. The main contributions of this paper are:

- A novel saturated stabilization controller with visual feedback for unicycle-type wheeled mobile robots.
- A rigorous theoretical validation of the proposed saturated controller guaranteeing global uniform asymptotic stability, supported by Lyapunov and non-autonomous cascade systems theory.
- An experimental comparison of the proposed visual controller concerning the controller reported in [35].

The remaining part of this article is organized as follows. Section II presents some preliminaries necessary for stability analysis. In Section III, the kinematic model is obtained, and the control aim is declared. The proposed saturated controller and the theoretical validation are presented in Section IV. In Section V, the controller chosen for experimental comparison, the description of the experimental platform, and the real-time experimental results are given. Finally, the work conclusions are reported in Section VI.

II. PRELIMINARIES

In this section, some useful lemmas are described to support the stability analysis of the proposed saturated controller described in Section IV.

Lemma 1 ([36]): If $\dot{f}(t) = \frac{d}{dt}f(t)$ is bounded for $t \in [0, \infty)$, then $f(t)$ is uniformly continuous for $t \in [0, \infty)$. $\square$

Lemma 2 ([37]): Let $\phi : \mathbb{R} \to \mathbb{R}$ be a uniformly continuous function on $[0, \infty)$. Suppose that $\lim_{t\to\infty} \int_0^t \phi(\tau)d\tau$ exists and is finite. Then, $\phi(t) \to 0$ as $t \to \infty$. $\square$

Lemma 3 ([36]): If a given differentiable function $f(t)$: $\mathbb{R}_+ \to \mathbb{R}$ has a finite limit as $t \to \infty$ and if $f(t)$ has a time derivative, defined as $\dot{f}(t)$, that can be written as the sum of two functions, denoted by $g_1(t)$ and $g_2(t)$, as follows

$$\dot{f}(t) = g_1(t) + g_2(t),$$

where $g_1(t)$ is a uniformly continuous function and

$$\lim_{t\to\infty} g_2(t) = 0,$$

then

$$\lim_{t\to\infty} \dot{f}(t) = 0, \quad \lim_{t\to\infty} g_1(t) = 0.$$

□

Lemma 4 ([37]): Consider the system

$$\dot{\boldsymbol{x}} = \boldsymbol{f}(t, \boldsymbol{x}) + \boldsymbol{g}(t, \boldsymbol{x}), \tag{1}$$

where $\boldsymbol{f} : [0, \infty) \times D \to \mathbb{R}^m$ and $\boldsymbol{g} : [0, \infty) \times D \to \mathbb{R}^m$ are piecewise continuous in t and locally Lipschitz in $\boldsymbol{x}$ on $[0, \infty) \times D$, and $D \subset \mathbb{R}^m$ is a domain that contains the origin $\boldsymbol{x} = \boldsymbol{0}$. This system can be considered as a perturbation of the nominal system

$$\dot{\boldsymbol{x}} = \boldsymbol{f}(t, \boldsymbol{x}).$$

Let $\boldsymbol{x} = \boldsymbol{0}$ be a uniformly asymptotically stable equilibrium point of the nominal system. Let $V(t, \boldsymbol{x})$ be a Lyapunov function of the nominal system that satisfies the inequalities

$$\begin{aligned} \alpha_1(\|\boldsymbol{x}\|) \le V(t, \boldsymbol{x}) &\le \alpha_2(\|\boldsymbol{x}\|), \\ \frac{\partial V}{\partial t} + \frac{\partial V}{\partial \boldsymbol{x}}\boldsymbol{f}(t, \boldsymbol{x}) &\le -\alpha_3(\|\boldsymbol{x}\|), \\ \left\| \frac{\partial V}{\partial \boldsymbol{x}} \right\| &\le \alpha_4(\|\boldsymbol{x}\|), \end{aligned}$$

in $[0, \infty) \times D$, where $D = \{\boldsymbol{x} \in \mathbb{R}^n | \|\boldsymbol{x}\| < r\}$ and $\alpha_i(\cdot)$, $i = 1, 2, 3, 4$, are class $\mathcal{K}$ functions. Suppose the perturbation term $\boldsymbol{g}(t, \boldsymbol{x})$ satisfies the uniform bound

$$\|\boldsymbol{g}(t, \boldsymbol{x})\| \le \delta < \frac{\sigma \alpha_3(\alpha_2^{-1}(\alpha_1(r)))}{\alpha_4(r)}$$

for all $t \ge 0$, all $\boldsymbol{x} \in D$, and some positive constant $\sigma < 1$. Then, for all $\|\boldsymbol{x}(t_0)\| < \alpha_2^{-1}(\alpha_1(r))$, the solution $\boldsymbol{x}(t)$ of the perturbed system (1) satisfies

$$\|\boldsymbol{x}(t)\| \le \beta(\|\boldsymbol{x}(t_0)\|, t - t_0), \quad \forall t_0 \le t < t_0 + T,$$

and

$$\|\boldsymbol{x}(t)\| \le \rho(\delta), \quad \forall t \ge t_0 + T,$$

for some class $\mathcal{KL}$ function β and some finite T, where ρ is a class $\mathcal{K}$ function of δ. □

Lemma 5 ([38]): Let be a nonlinear time-varying system given by

$$\Sigma_1 : \dot{\boldsymbol{x}}_1 = \boldsymbol{f}_1(t, \boldsymbol{x}_1) + \boldsymbol{g}(t, \boldsymbol{x})\boldsymbol{x}_2, \tag{2}$$

$$\Sigma_2 : \dot{\boldsymbol{x}}_2 = \boldsymbol{f}_2(t, \boldsymbol{x}_2), \tag{3}$$

where $\boldsymbol{x}_1 \in \mathbb{R}^n$, $\boldsymbol{x}_2 \in \mathbb{R}^m$, $\boldsymbol{x} := [\boldsymbol{x}_1^T,\ \boldsymbol{x}_2^T]^T$. The functions $\boldsymbol{f}_1(t, \boldsymbol{x}_1)$, $\boldsymbol{f}_2(t, \boldsymbol{x}_2)$ and $\boldsymbol{g}(t, \boldsymbol{x})$ are continuous in their arguments, locally Lipschitz in $\boldsymbol{x}$, uniformly in t, and $\boldsymbol{f}_1(t, \boldsymbol{x}_1)$ is continuously differentiable in both arguments. Also, it is assumed that there exists a nondecreasing function $G(\cdot)$ such that,

$$\|\boldsymbol{g}(t, \boldsymbol{x})\| \le G(\|\boldsymbol{x}\|).$$

If the systems

$$\dot{\boldsymbol{x}}_1 = \boldsymbol{f}_1(t, \boldsymbol{x}_1), \tag{4}$$

$$\dot{\boldsymbol{x}}_2 = \boldsymbol{f}_2(t, \boldsymbol{x}_2), \tag{5}$$

are uniformly globally asymptotically stable and the solutions of (2) and (3) are globally uniformly bounded, then (2) and (3) are uniformly globally asymptotically stable. □

III. KINEMATIC MODEL AND CONTROL OBJECTIVE

This work addresses the problem of positioning a unicycle-type mobile robot using visual information as feedback signals. The system is composed of a unicycle-type wheeled vehicle that is equipped with a camera. Figure 1 shows the scheme of the system considered. The camera has a fixed orthogonal coordinate system denoted by F. The origin O of F is located in the optical center of the camera. The Z-axis of F passes through the middle of the wheel axis and is orthogonal to the horizontal plane. The X-axis of F coincides with the direction of the camera optical axis and is aligned to the robot front. Besides, the desired pose of the camera is established by the coordinate reference frame F^*.

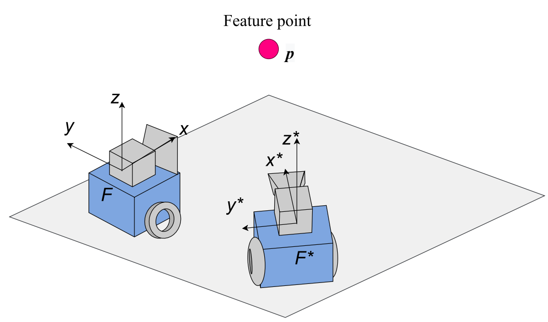

FIGURE 1. Coordinate system.

The visual feedback is performed by identifying a static feature point $\boldsymbol{P}$ in the scene. The coordinates of $\boldsymbol{P}$ in the reference frame F are denoted by $\boldsymbol{P} = [X, Y, Z]^T$, whereas $\boldsymbol{P}^* = [X^*, Y^*, Z^*]^T$ are the coordinates of the same point $\boldsymbol{P}$ in the desired reference frame F^*.

Moreover, the homogeneous image pixel coordinates are given by

$$\boldsymbol{p} = [1, u, v]^T, \quad \boldsymbol{p}^* = [1, u^*, v^*]^T. \tag{6}$$

The coordinates $\boldsymbol{P}$ and $\boldsymbol{P}^*$ are related with the image pixel coordinates $\boldsymbol{p}$ and $\boldsymbol{p}^*$ through a pinhole camera model as

$$\boldsymbol{p} = \frac{1}{X}A\boldsymbol{P}, \quad \boldsymbol{p}^* = \frac{1}{X}A\boldsymbol{P}^*, \tag{7}$$

where $A \in \mathbb{R}^3$ is the intrinsic parameters matrix of the camera defined as

$$A = \begin{bmatrix} 1 & 0 & 0 \\ u_0 & \alpha_u & 0 \\ v_0 & 0 & \alpha_v \end{bmatrix}, \tag{8}$$

with u_0, v_0 denoting principal point coordinates, and α_u, α_v representing the scale factors in image u and v axes, respectively [39].

To simplify the analysis, the vectors $\boldsymbol{m}$ and $\boldsymbol{m}^* \in \mathbb{R}^3$ are introduced. These vectors represent the normalized image coordinates of the object of interest, define as

$$\boldsymbol{m} = [1, y, z]^T = \tfrac{1}{X}\boldsymbol{P}, \quad \boldsymbol{m}^* = [1, y^*, z^*]^T = \tfrac{1}{X}\boldsymbol{P}^*. \tag{9}$$

By using (7) and (9), the next expression is obtained:

$$\boldsymbol{m} = A^{-1}\boldsymbol{p}, \quad \boldsymbol{m}^* = A^{-1}\boldsymbol{p}^*. \tag{10}$$

A rigid motion is described by a pure translation together with a pure rotation. Specifically for this work, the rotation matrix $R \in \mathbb{R}^{3\times 3}$ specifies the orientation of the reference frame F^* concerning F, and $T \in \mathbb{R}^3$ is the vector from the origin of frame F to the origin of F^*. Therefore, considering that the movement of the camera attached to the vehicle is restricted to the XY plane, the vector T and the matrix R are defined by

$$R = \begin{bmatrix} \cos(\tilde{\theta}) & -\sin(\tilde{\theta}) & 0 \\ \sin(\tilde{\theta}) & \cos(\tilde{\theta}) & 0 \\ 0 & 0 & 1 \end{bmatrix}, \quad \boldsymbol{T} = \begin{bmatrix} t_x \\ t_x \\ 0 \end{bmatrix}, \tag{11}$$

where $\tilde{\theta} = \theta^* - \theta$ with θ^* and θ denote the desired and actual orientation of the camera, respectively. The estimation of the camera orientation can be obtained using different algorithms as in [39], homography techniques [40], [41], or odometry [26], [42]. Note that $\tilde{\theta} = 0$ and $\boldsymbol{T} = \boldsymbol{0}$ imply that the coordinate frame of the camera F coincides with the desired one F^*.

Also, the well-known geometric properties define the relationship of $\boldsymbol{P}$ with $\boldsymbol{P}^*$ given by

$$\boldsymbol{P} = R\boldsymbol{P}^* + \boldsymbol{T},$$

thus, the next expression is obtained

$$\begin{bmatrix} X \\ Y \\ Z \end{bmatrix} = \begin{bmatrix} X^*\cos(\tilde{\theta}) - Y^*\sin(\tilde{\theta}) + t_x \\ X^*\sin(\tilde{\theta}) + Y^*\cos(\tilde{\theta}) + t_y \\ Z^* \end{bmatrix} \tag{12}$$

and, the following equations are derived from (12)

$$\frac{Y}{X} = \frac{X^*\sin(\tilde{\theta}) + Y^*\cos(\tilde{\theta}) + t_y}{X^*\cos(\tilde{\theta}) - Y^*\sin(\tilde{\theta}) + t_x}, \tag{13}$$

$$\frac{Z}{X} = \frac{Z^*}{X^*\cos(\tilde{\theta}) - Y^*\sin(\tilde{\theta}) + t_x}. \tag{14}$$

By using the definitions in (9), (13) and (14) can be rewritten as

$$y = \frac{\sin(\tilde{\theta}) + y^*\cos(\tilde{\theta}) + \frac{t_y}{X^*}}{\cos(\tilde{\theta}) - y^*\sin(\tilde{\theta}) + \frac{t_x}{X^*}},$$

$$z = \frac{z^*}{\cos(\tilde{\theta}) - y^*\sin(\tilde{\theta}) + \frac{t_x}{X^*}}.$$

Besides, considering that $z \neq 0$ and after going some algebraic manipulations is possible to obtain

$$y\frac{z^*}{z} = \sin(\tilde{\theta}) + y^*\cos(\tilde{\theta}) + \frac{t_y}{X^*}, \tag{15}$$

$$\frac{z^*}{z} = \cos(\tilde{\theta}) - y^*\sin(\tilde{\theta}) + \frac{t_x}{X^*}. \tag{16}$$

Note that if $y/z = y^*/z^*$, $1/z = 1/z^*$ and $\tilde{\theta} = 0$ then $\boldsymbol{T} = 0$, and therefore $F = F^*$.

Based on classical image-based visual servo control [43], the vector $\boldsymbol{s}$ is defined as

$$\boldsymbol{s} = [y, z]^T = \begin{bmatrix} \frac{Y}{X} & \frac{Z}{X} \end{bmatrix}, \tag{17}$$

where y and z are the normalized image pixel coordinates in (9). Taking the time derivative of $\boldsymbol{s}$, the relation of the camera spacial velocity with the feature point velocity is established as

$$\dot{\boldsymbol{s}} = L_s\mathbf{v}_c, \tag{18}$$

where $\mathbf{v}_c = [v_{cx}\ v_{cy}\ v_{cz}\ \omega_{cx}\ \omega_{cy}\ \omega_{cz}]^T$ is the camera velocity screw, and $L_s \in \mathbb{R}^{2\times 6}$ is the interaction matrix related to $\boldsymbol{s}$ given by

$$L_s = \begin{bmatrix} \frac{1}{X} & 0 & \frac{y}{X} & z & yz & -(1+y^2) \\ 0 & -\frac{1}{X} & \frac{z}{X} & y & 1+z^2 & -yz \end{bmatrix}. \tag{19}$$

Considering that there is no relative movement between the robot and the camera, the following assumption is established as

$$Z = Z^*. \tag{20}$$

Furthermore, the movement restrictions of the unicycle-type mobile robot produce a reduced model of (18) given by

$$\dot{\boldsymbol{s}} = L\mathbf{v}, \tag{21}$$

where the simplified interaction matrix is defined as

$$L = \begin{bmatrix} \frac{y}{X} & -(1+y^2) \\ \frac{z}{X} & -yz \end{bmatrix}, \tag{22}$$

and $\mathbf{v} = [V\ W]^T \in \mathbb{R}^2$, with $V = v_{cx}$ the linear velocity and $W = \omega_z$ the angular velocity applied to the mobile robot.

To introduce the kinematic model the following state variables are used

$$\rho_1 = \frac{y}{z}, \quad \rho_2 = \frac{1}{z}, \tag{23}$$

then, the time derivatives are computed and some substitutions are done to obtain kinematics model,

$$\dot{\rho}_1 = -\rho_2 W, \tag{24}$$

$$\dot{\rho}_2 = -\frac{1}{X}V + \rho_1 W. \tag{25}$$

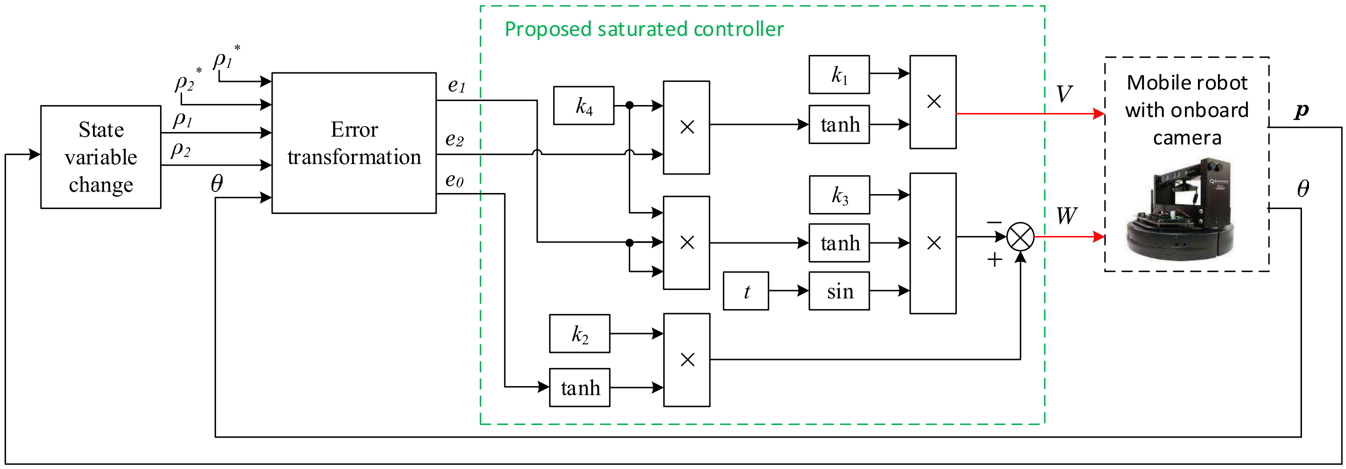

FIGURE 2. Saturated controller implementation described in a block diagram.

Let ρ_1^* and ρ_2^* be constant desired values defined as $\rho_1^* = y^*/z^*$ and $\rho_2^* = 1/z^*$. From (15) and (16), it is clear if $\rho_1(t) \to \rho_1^*$, $\rho_2(t) \to \rho_2^*$ and $\tilde{\theta} \to 0$ then, the F and F^* reference frames are coincident.

Thus, the control objective consists in design saturated control signals $\mathbf{v} = [V(t)\ W(t)]^T$ such that

$$\rho_1(t) \to \rho_1^*, \quad \rho_2(t) \to \rho_2^*, \text{ and } \tilde{\theta}(t) \to 0, \tag{26}$$

guaranteeing

$$|W(t)| \leq W_{\max}, \quad |V(t)| \leq V_{\max}, \quad \forall\ t \geq 0, \tag{27}$$

where $W_{\max}$ and $V_{\max}$ are the saturation levels given as arbitrary constants.

IV. SATURATED CONTROL LAW

In order to simplify the controller design, the error signals e_0, e_1, and e_2 are defined as

$$e_0 = \tilde{\theta}, \tag{28}$$

$$\begin{bmatrix} e_1 \\ e_2 \end{bmatrix} = \begin{bmatrix} \rho_1 \\ \rho_2 \end{bmatrix} - \begin{bmatrix} \cos(\tilde{\theta}) & -\sin(\tilde{\theta}) \\ \sin(\tilde{\theta}) & \cos(\tilde{\theta}) \end{bmatrix} \begin{bmatrix} \rho_1^* \\ \rho_2^* \end{bmatrix}. \tag{29}$$

The open-loop error dynamics are obtained by substituting (24) and (25) in the time derivative of the error signals e_0, e_1, and e_2 as

$$\begin{bmatrix} \dot{e}_0 \\ \dot{e}_1 \\ \dot{e}_2 \end{bmatrix} = \begin{bmatrix} W \\ -e_2 W \\ -\frac{1}{Z} V + e_1 W \end{bmatrix}. \tag{30}$$

Note that the open-loop error system is obtained considering that ρ_1^*, ρ_2^*, and θ^* are constants, which agree with the problem definition of moving the robot to a fixed desired pose.

The proposed saturated stabilization controller is inspired by the work reported in [44]. The properties of the hyperbolic tangent function have been taken into account to design the visual controller with bounded inputs. Thus, the proposed controller is defined by

$$\begin{bmatrix} V \\ W \end{bmatrix} = \begin{bmatrix} k_1 \tanh(k_4 e_2) \\ -k_2 \tanh(e_0) + k_3 \tanh(k_4 e_1^2) \sin(t) \end{bmatrix}, \tag{31}$$

where k_1, k_2, k_3, and k_4 are strictly positive control gains. Note that the term $k_3 \tanh(k_4 e_1^2) \sin(t)$ prevents the dynamics of $e_1(t)$ from being uncontrollable when $W(t) = 0$. In consequence, the upper symmetric bounds of the control law (31) are given by

$$\begin{aligned} |V(t)| &\leq V_{\max} = k_1, \\ |W(t)| &\leq W_{\max} = k_2 + k_3, \end{aligned} \tag{32}$$

where the bounds $|\tanh(x)|, |\sin(x)| \leq 1 \quad \forall \quad x \in \mathbb{R}$ have been used. The controller structure can be seen in the block diagram given in Figure 2.

Substituting the control law (31) in the open-loop error system (30), the following closed-loop error system is obtained

$$\dot{e}_0 = -k_2 \tanh(e_0) + k_3 \tanh(k_4 e_1^2) \sin(t), \tag{33}$$

$$\begin{bmatrix} \dot{e}_1 \\ \dot{e}_2 \end{bmatrix} = \begin{bmatrix} -e_2\ W \\ -\frac{k_1}{Z} \tanh(k_4 e_2) + e_1 W \end{bmatrix}, \tag{34}$$

which is a cascade non-autonomous nonlinear system with the structure of (2) - (3), where $x_1 = e_0$, $\boldsymbol{x}_2 = [e_1\ e_2]^T$,

$$\begin{aligned} f_1(x_1, t) &= -k_2 \tanh(e_0), \\ \boldsymbol{f}_2(\boldsymbol{x}_2, t) &= \begin{bmatrix} -e_2\ W \\ -\frac{k_1}{Z} \tanh(k_4 e_2) + e_1 W \end{bmatrix}, \\ g(t, \boldsymbol{x}) &= \begin{bmatrix} \frac{k_3 \tanh(k_4 e_1^2) \sin(t)}{e_1} & 0 \end{bmatrix}. \end{aligned}$$

Proposition 1: The equilibrium point $\boldsymbol{x} = [e_0\ e_1\ e_2]^T = \mathbf{0}$ of the cascade non-autonomous nonlinear system (33)-(34) is globally uniformly asymptotically stable.

Proof: First, the following non-negative function is proposed

$$V_1 = \frac{1}{2} e_1^2 + \frac{1}{2} e_2^2, \tag{35}$$

where the time derivative is given by

$$\dot{V}_1 = e_1\dot{e}_1 + e_2\dot{e}_2. \tag{36}$$

By substituting $\dot{e}_1$ and $\dot{e}_2$ from the equation (34), it is possible to obtain

$$\dot{V}_1 = -\frac{k_1}{Z}e_2 \tanh(k_4 e_2). \tag{37}$$

Since $e_2 \tanh(e_2) \geq 0$ for all $t \geq 0$, the inequality $\dot{V}_1 \leq 0$ for all $t \geq 0$ is satisfied. From the equations (35) and (37), it is clear that $e_1(t), e_2(t) \in L_\infty$. Since the control inputs V and W are bounded as stated in (32), then V, $W \in L_\infty$. Also, $\dot{e}_0$, $\dot{e}_1$, $\dot{e}_2 \in L_\infty$ based on the equations (33)-(34) and the fact that the sine and hyperbolic tangent functions are bounded. Besides, $e_0(t), e_1(t), e_2(t)$ are uniformly continuous functions by using Lemma 1. Calculating the derivative of (31) and by the facts that have been determined, it can be shown that $\dot{V}(t)$, $\dot{W}(t) \in L_\infty$ and, therefore, $V(t)$, $W(t)$ are uniformly continuous.

Integrating both sides of (37), the following expression is obtained

$$-\int_0^\infty \dot{V}_1(t)dt = \frac{k_1}{Z}\int_0^\infty e_2(t)\tanh(k_4 e_2(t))dt. \tag{38}$$

Evaluating the definite integral from the left side, we get

$$\int_0^\infty e_2(t)\tanh(k_4 e_2(t))dt \leq \frac{ZV_1(0)}{k_1} < \infty. \tag{39}$$

Thus, knowing that e_2 is a uniformly continuous function and that the integral (39) exists and is finite, the following limit

$$\lim_{t\to\infty} e_2(t) = 0 \tag{40}$$

is guaranteed by using Lemma 2.

Now, the time derivative of the product $e_1(t)e_2(t)$ is calculated, obtaining

$$\frac{d}{dt}(e_1 e_2) = (\dot{e}_1 e_2 - \tfrac{k_1}{Z}\tanh(k_4 e_2)e_1) + [e_1^2 W]. \tag{41}$$

Since $\lim_{t\to\infty} e_2(t) = 0$ has been proved, and the term in brackets in (41) is uniformly continuous, it is possible to invoke Lemma 3 to conclude that

$$\lim_{t\to\infty}\frac{d}{dt}(e_1(t)e_2(t)) = 0 \quad \text{and} \lim_{t\to\infty} e_1^2(t)W(t) = 0. \tag{42}$$

From this last result, it is clear that either $\lim_{t\to\infty} e_1^2(t) = 0$, $\lim_{t\to\infty} W(t) = 0$, or both are zero. Therefore the limit (42) implies

$$\lim_{t\to\infty} e_1(t)W(t) = 0, \tag{43}$$

since the limit of a product is equal to the product of the limits. Besides, using (31), (34), (40), and (43), the next limits are proved

$$\lim_{t\to\infty} V(t) = 0, \quad \lim_{t\to\infty}\dot{e}_1(t) = 0, \text{ and } \lim_{t\to\infty}\dot{e}_2(t) = 0. \tag{44}$$

Subsequently, the temporal derivative of the product $e_1(t)W(t)$ is calculated, and then the equations (30) and (31) are used to yield

$$\begin{aligned}\frac{d}{dt}(e_1 W) = {} & [k_3 e_1 \tanh(k_4 e_1^2)\cos(t)] - k_2 \operatorname{sech}^2(e_0)e_1 W \\ & + \dot{e}_1(W + 2k_3 k_4 e_2^2 \operatorname{sech}^2(k_4 e_1^2)\sin(t)).\end{aligned} \tag{45}$$

Since the term in brackets of (45) is uniformly continuous and $\lim_{t\to\infty}\dot{e}_1(t) = 0$ and $\lim_{t\to\infty} e_1(t)\,W = 0$, Lemma 3 can be used to state that

$$\lim_{t\to\infty}\frac{d}{dt}(e_1(t)W(t)) = 0, \tag{46}$$

and

$$\lim_{t\to\infty} k_3 e_1 \tanh(k_4 e_1^2)\cos(t) = 0. \tag{47}$$

Hence, we can conclude that

$$\lim_{t\to\infty} e_1(t) = 0. \tag{48}$$

In order to show that the equilibrium point $e_0 = 0$ is globally uniformly bounded, consider the no negative function

$$V_2 = \ln(\cosh(e_0)),$$

whose time derivative is given by

$$\dot{V}_2 = \frac{\sinh(e_0)}{\cosh(e_0)}\dot{e}_0 = \tanh(e_0)\dot{e}_0,$$

substituting the definition of $\dot{e}_0$ in (33) and using the fact $|k_3 \tanh(k_4 e_1^2)\sin(t)| \leq k_3, \ \forall t \geq 0$, the derivative of V_2 can be upper bounded as

$$\dot{V}_2 \leq -k_2 \tanh^2(e_0) + k_3.$$

Since conditions of Lemma 4 are satisfied, the fact that $e_0(t) \in L_\infty$ is proven. Besides, if the term $k_3 \tanh(k_4 e_1^2)\sin(t)$ is omitted in (33), the system is globally uniformly asymptotically stable. Thus, the Lemma 5 conditions are satisfied, and the equilibrium point $\boldsymbol{x} = [e_0\ e_1\ e_2]^T = \mathbf{0}$ is globally uniformly asymptotically stable, and the proof is concluded. □

V. EXPERIMENTAL VALIDATION

A. CONTROLLER FOR COMPARISON

In order to compare the new proposal of control, the following smooth feedback control law reported in [35] has been selected. The linear and angular velocities defined as control inputs are given by

$$\begin{bmatrix} V \\ W \end{bmatrix} = \begin{bmatrix} \Gamma\boldsymbol{r}, \\ -k_0 e_0 + \lambda e^{\gamma t} \end{bmatrix}, \tag{49}$$

where the state variable $\boldsymbol{r}$ is defined as

$$\boldsymbol{r} = \begin{bmatrix} e_2 \\ e_1\, e^{\gamma t} \end{bmatrix}, \tag{50}$$

$\Gamma = [k_1\ k_2] \in \mathbb{R}^{1\times 2}$ is a control gain matrix, $k_0, \gamma \in \mathbb{R}$ are positive constants, and $\lambda \in \mathbb{R}$ is a nonzero constant.

B. DESCRIPTION OF THE EXPERIMENTAL PLATFORM

All the elements that compose the experimental platform are shown in Figure 3. The mobile robot used to implement the controllers is the Qbot 2 manufactured by *Quanser*. The robot has a *Microsoft Kinect* device on board. This device has two cameras, the first one is an RGB camera, and the other is an IR depth camera, both with a resolution of 640×480 [pixels]. In this work, the robot orientation is estimated by using the odometry system of the Qbot 2.

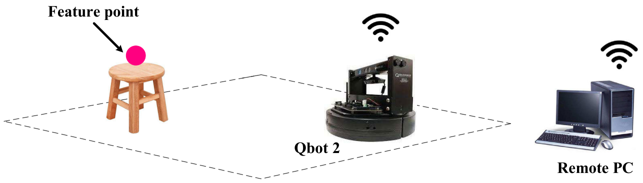

FIGURE 3. Experimental platform.

The controllers were programmed in *Matlab-Simulink* using the *QUARC Real-Time* library. The image processing used to identify and extract the coordinates in the image plane of the feature point was implemented using the computer vision toolbox. The frame rate of the image acquisition was set at 10 frames per second. A magenta color ball was selected as the feature point because this object presents high contrast with the other objects in the experimental area. Thus, the feature point position in the image plane $\boldsymbol{p}$ was obtained using image processing based on color and shape. Two experiments were carried out, one applying the smooth feedback controller and the other one using the proposed saturated controller. In both experiments, just a single feature point was considered, and the experimental time was set at 35 seconds.

C. EXPERIMENTAL RESULTS

The camera intrinsic parameters used in obtaining the normalized coordinates of the image in (9) were taken from the literature [45]. Specifically, $\alpha_u = 834.01$, $\alpha_v = 839.85$, $u_0 = 305.51$ and $v_0 = 240.09$.

The control gains for the smooth feedback controller were set by a trial and error procedure, with the following values

$$k_0 = 0.35,\; k_1 = 0.29,\; k_2 = -0.0414,$$
$$\gamma = 0.01, \qquad \lambda = 0.01.$$

Similarly, the gains for the proposed saturated controller were selected by a trial and error procedure to establish velocities bounds that ensure that the feature point remains in the camera's field of view. The resulting values were $V_{\max} = 0.25$ [m/s] and $W_{\max} = 0.269$ [rad/s], with

$$k_1 = 0.25, \quad k_2 = 0.225, \quad k_3 = 0.044, \quad k_4 = 2.5.$$

It is clear from (7) and (12) that the desired pose of the camera can be established uniquely by defining the pixel coordinates in the image and the orientation of the unicycle-type mobile robot when $z = 0$. Thus, the desired position of the feature point and the desired orientation were defined as

$$p^* = \begin{bmatrix} 324 & 124 \end{bmatrix} \text{[pixel]}, \quad \theta^* = 1.5 \text{ [rad]}.$$

Figures 4 - 8 present the experimental results. The paths of the feature point in the image plane with both controllers are depicted in Figure 4. Observe how the proposed controller allows reaching a position closer to the desired one than the smooth feedback controller. In addition, both controllers have a similar path shape. The time evolution of the pixel coordinates of the feature point is given in Figure 5. It is important to highlight the precision difference of the proposed control compared to the smooth feedback controller. For the $v(t)$ pixel coordinate, the performance is similar in both controllers. However, for the $u(t)$ pixel coordinate, the desired value is reached using the proposed controller, while a considerable stationary state error is obtained using the smooth feedback controller. Similarly, Figure 6 shows the orientation angle $\theta(t)$ described by the robot. The proposed controller keeps the actual orientation closer to the desired value than the comparison controller. The transformed error signals $e_0(t)$, $e_1(t)$,

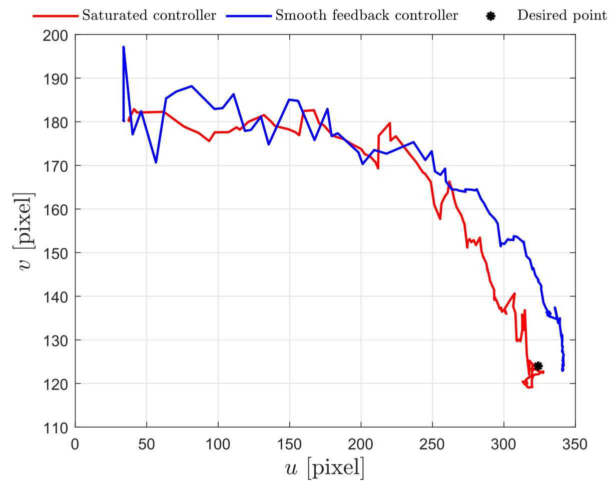

FIGURE 4. Experimental results: Image path of the feature point.

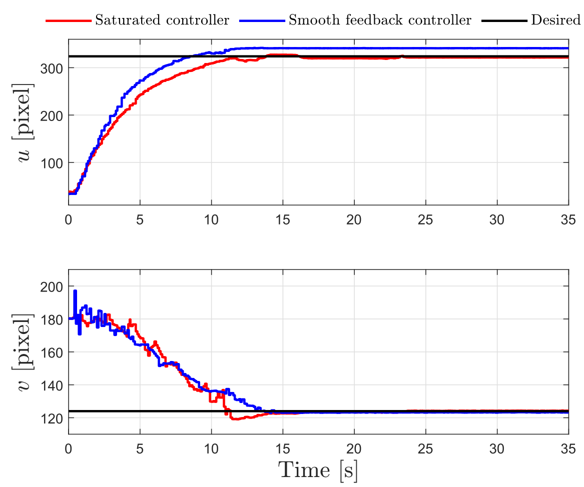

FIGURE 5. Experimental results: Time evolution of pixel coordinates.

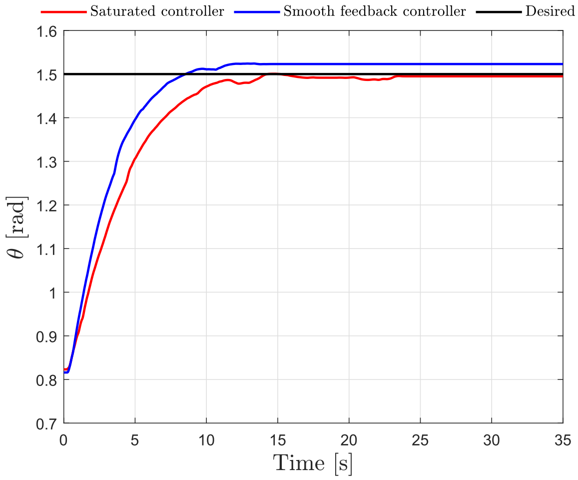

FIGURE 6. **Experimental results: Time evolution of robot orientation.**

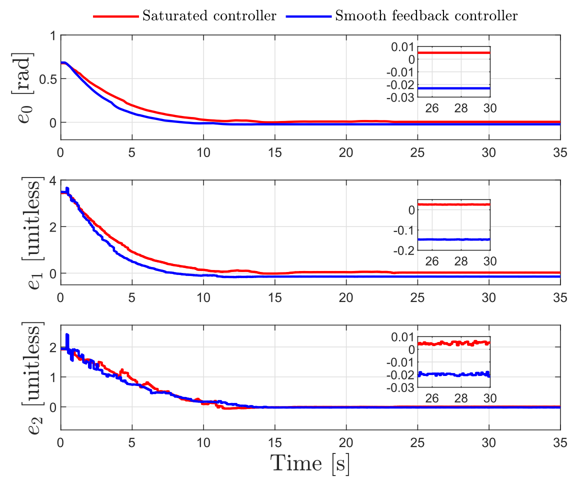

FIGURE 7. **Experimental results: Time evolution of errors signals.**

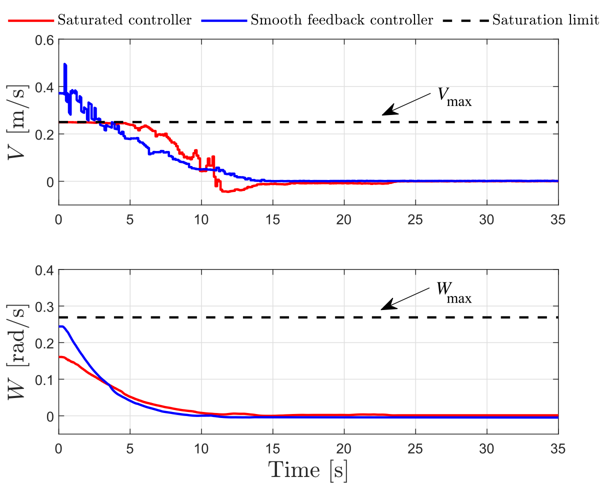

FIGURE 8. **Experimental results: Control signals.**

and $e_2(t)$ are depicted in Figure 7. In all error signals, the proposed controller achieves a smaller error magnitude. Finally, Figure 8 presents the control inputs $V(t)$ and $W(t)$ obtained with the tested controllers. Note that the proposed controller maintains the control actions limited for all the experiment time. Specifically, the linear velocity $V(t)$ remains close to the saturation bound during the first five seconds.

Additionally, to present a quantitative performance analysis, the RMS values for the image pixel coordinates errors $\tilde{u} = u - u^*$ and $\tilde{v} = v - v^*$ and the orientation error $\tilde{\theta}$ were computed with each tested controller. The results are given in Table 1. As can be seen, the proposed saturated controller reaches the closest position to the desired one, whereas the control action is kept bounded. Besides, the proposed controller performs better orientation tracking.

TABLE 1. **Experimental results: RMS values of the pose error calculated in the time interval 25 [s] $\leq t \leq$ 35 [s].**

	RMS($\tilde{u}$) [pixel]	RMS($\tilde{v}$) [pixel]	RMS($\tilde{\theta}$) [rad]
Smooth feedback controller	17.169	0.772	0.023
Saturated controller	**2.513**	**0.222**	**0.005**

VI. CONCLUSION

In this paper, a novel saturated visual control strategy for nonholonomic mobile robots was presented. The proposed controller guarantees that the robot achieves the desired pose. The design of the controller provides bounded input signals for the linear and angular velocities. These saturation limits allow setting the maximum camera movement velocities either according to the physical characteristics of the actuators or the needs of the assigned task. A rigorous theoretical validation was presented. The closed-loop system was dealt with as a cascade non-autonomous system, and global uniform asymptotic stability was guaranteed. An experimental comparison was carried out with a similar visual control strategy with unsaturated control inputs. The experimental results obtained using the proposed method showed better performance, reducing the position errors. Different issues can be studied to improve the performance of the analyzed system. For example, more robust computer vision techniques can be implemented to identify the feature point in the scene. In the same way, the orientation estimation of the vehicle concerning the desired pose can be obtained using methods other than odometry. Finally, the problem of unified control of regulation and trajectory tracking for nonholonomic vehicles with input constraints is an interesting research topic to be studied.

REFERENCES

[1] Z. Ma and J. Su, "Robust uncalibrated visual servoing control based on disturbance observer," *ISA Trans.*, vol. 59, pp. 193–204, Nov. 2015.

[2] H. Xie and A. F. Lynch, "State transformation-based dynamic visual servoing for an unmanned aerial vehicle," *Int. J. Control*, vol. 89, no. 5, pp. 892–908, May 2016.

[3] T. Li and H. Zhao, "Global finite-time adaptive control for uncalibrated robot manipulator based on visual servoing," *ISA Trans.*, vol. 68, pp. 402–411, May 2017.

[4] J. Gao, X. An, A. Proctor, and C. Bradley, "Sliding mode adaptive neural network control for hybrid visual servoing of underwater vehicles," *Ocean Eng.*, vol. 142, pp. 666–675, Sep. 2017.

[5] T. Dewi, P. Risma, Y. Oktarina, and S. Muslimin, "Visual servoing design and control for agriculture robot; a review," in *Proc. Int. Conf. Electr. Eng. Comput. Sci. (ICECOS)*, Oct. 2018, pp. 57–62.

[6] D. Zheng, H. Wang, J. Wang, X. Zhang, and W. Chen, "Toward visibility guaranteed visual servoing control of quadrotor UAVs," *IEEE/ASME Trans. Mechatronics*, vol. 24, no. 3, pp. 1087–1095, Jun. 2019.

[7] F. Xu, H. Wang, J. Wang, K. W. S. Au, and W. Chen, "Underwater dynamic visual servoing for a soft robot arm with online distortion correction," *IEEE/ASME Trans. Mechatron.*, vol. 24, no. 3, pp. 979–989, Jun. 2019.

[8] Y. Zhang, C. Hua, Y. Li, and X. Guan, "Adaptive neural networks-based visual servoing control for manipulator with visibility constraint and deadzone input," *Neurocomputing*, vol. 332, pp. 44–55, Mar. 2019.

[9] W. Zhao, H. Liu, F. L. Lewis, K. P. Valavanis, and X. Wang, "Robust visual servoing control for ground target tracking of quadrotors," *IEEE Trans. Control Syst. Technol.*, vol. 28, no. 5, pp. 1980–1987, Sep. 2020.

[10] J. Dong and J. Zhang, "A new image-based visual servoing method with velocity direction control," *J. Franklin Inst.*, vol. 357, no. 7, pp. 3993–4007, May 2020.

[11] K. Wang, Y. Liu, and L. Li, "Visual servoing trajectory tracking of nonholonomic mobile robots without direct position measurement," *IEEE Trans. Robot.*, vol. 30, no. 4, pp. 1026–1035, Aug. 2014.

[12] H. Aliakbarpour, O. Tahri, and H. Araujo, "Visual servoing of mobile robots using non-central catadioptric cameras," *Robot. Auton. Syst.*, vol. 62, pp. 1613–1622, Nov. 2014.

[13] X. Zhang, Y. Fang, B. Li, and J. Wang, "Visual servoing of nonholonomic mobile robots with uncalibrated camera-to-robot parameters," *IEEE Trans. Ind. Electron.*, vol. 64, no. 1, pp. 390–400, Jan. 2017.

[14] B. Li, X. Zhang, Y. Fang, and W. Shi, "Visual servoing of wheeled mobile robots without desired images," *IEEE Trans. Cybern.*, vol. 49, no. 8, pp. 2835–2844, Aug. 2019.

[15] Y. Qiu, B. Li, W. Shi, and Y. Chen, "Concurrent-learning-based visual servo tracking and scene identification of mobile robots," *Assem. Autom.*, vol. 39, no. 3, pp. 460–468, Aug. 2019.

[16] Y. Qiu, B. Li, W. Shi, and X. Zhang, "Visual servo tracking of wheeled mobile robots with unknown extrinsic parameters," *IEEE Trans. Ind. Electron.*, vol. 66, no. 11, pp. 8600–8609, Nov. 2019.

[17] M. Dirik, O. Castillo, and A. F. Kocamaz, "Visual-servoing based global path planning using interval type-2 fuzzy logic control," *Axioms*, vol. 8, no. 2, pp. 1–16, May 2019.

[18] F. Wang, Y. Qin, F. Guo, B. Ren, and J. T. W. Yeow, "Adaptive visually servoed tracking control for wheeled mobile robot with uncertain model parameters in complex environment," *Complexity*, vol. 2020, pp. 1–13, Dec. 2020.

[19] X. Zhang, Y. Fang, and N. Sun, "Visual servoing of mobile robots for posture stabilization: From theory to experiments," *Int. J. Robust Nonlinear Control*, vol. 25, no. 1, pp. 1–15, 2015.

[20] Q. Lu, L. Yu, D. Zhang, and X. Zhang, "Simultaneous tracking and regulation visual servoing of wheeled mobile robots with uncalibrated extrinsic parameters," *Int. J. Syst. Sci.*, vol. 49, no. 1, pp. 217–229, Jan. 2018.

[21] X. Liang, H. Wang, Y.-H. Liu, W. Chen, and Z. Jing, "Image-based position control of mobile robots with a completely unknown fixed camera," *IEEE Trans. Autom. Control*, vol. 63, no. 9, pp. 3016–3023, Sep. 2018.

[22] B. Li, X. Zhang, Y. Fang, and W. Shi, "Visual servo regulation of wheeled mobile robots with simultaneous depth identification," *IEEE Trans. Ind. Electron.*, vol. 65, no. 1, pp. 460–469, Jan. 2018.

[23] R. S. Sharma, S. Shukla, L. Behera, and V. K. Subramanian, "Position-based visual servoing of a mobile robot with an automatic extrinsic calibration scheme," *Robotica*, vol. 38, no. 5, pp. 831–844, May 2020.

[24] Y. Lin and K. Xing, "Visual servo optimization stabilization of nonholonomic mobile robots based on control Lyapunov functions," *Meas. Control*, vol. 53, nos. 9–10, pp. 1825–1831, Nov. 2020.

[25] Y. Huang and J. Su, "Robust uncalibrated visual stabilization for nonholonomic mobile robots," *Adv. Robot.*, vol. 34, no. 6, pp. 388–399, Mar. 2020.

[26] Q. Lu, Z. Li, L. Yu, and C.-Y. Su, "Adaptive visual regulation of wheeled mobile robots: A switching approach," *J. Intell. Robotic Syst.*, vol. 98, no. 2, pp. 345–358, May 2020.

[27] C.-L. Hwang, H.-M. Wu, and W.-H. Hung, "Software/hardware-based hierarchical finite-time sliding-mode control with input saturation for an omnidirectional autonomous mobile robot," *IEEE Access*, vol. 7, pp. 90254–90267, 2019.

[28] H. Huang, J. Zhou, Q. Di, J. Zhou, and J. Li, "Robust neural network–based tracking control and stabilization of a wheeled mobile robot with input saturation," *Int. J. Robust Nonlinear Control*, vol. 29, no. 2, pp. 375–392, Jan. 2019.

[29] K. Liu, H. Ji, and Y. Zhang, "Extended state observer based adaptive sliding mode tracking control of wheeled mobile robot with input saturation and uncertainties," *Proc. Inst. Mech. Eng., C, J. Mech. Eng. Sci.*, vol. 233, no. 15, pp. 5460–5476, Aug. 2019.

[30] P. Lu, W. Yu, G. Chen, and X. Yu, "Leaderless consensus of ring-networked mobile robots via distributed saturated control," *IEEE Trans. Ind. Electron.*, vol. 67, no. 12, pp. 10723–10731, Dec. 2020.

[31] J. Moreno-Valenzuela, L. Montoya-Villegas, R. Pérez-Alcocer, and J. Sandoval, "A family of saturated controllers for UWMRs," *ISA Trans.*, vol. 100, pp. 495–509, May 2020.

[32] X. Li and M. Wang, "Consensus control for wheeled mobile robots under input saturation constraint," *IEEE Access*, vol. 8, pp. 177125–177130, 2020.

[33] R. Wang, X. Zhang, Y. Fang, and B. Li, "Visual servoing of mobile robots with input saturation at kinematic level," in *Image and Graphics*, vol. 10666, Y. Zhao, X. Kong, and D. Taubman. Cham, Switzerland: Springer, Sep. 2017, pp. 432–442.

[34] R. Wang, X. Zhang, and Y. Fang, "Visual tracking of mobile robots with both velocity and acceleration saturation constraints," *Mech. Syst. Signal Process.*, vol. 150, Mar. 2021, Art. no. 107274.

[35] X. Zhang, Y. Fang, and X. Liu, "Motion-estimation-based visual servoing of nonholonomic mobile robots," *IEEE Trans. Robot.*, vol. 27, no. 6, pp. 1167–1175, Dec. 2011.

[36] W. E. Dixon, A. Behal, D. M. Dawson, and S. P. Nagarkatti, *Nonlinear Control of Engineering Systems*. Boston, MA, USA: Birkhäuser Basel, 2003.

[37] H. K. Khalil, *Nonlinear Systems*. Upper Saddle River, NJ, USA: Prentice-Hall, 2002.

[38] E. Panteley and A. Loría, "Growth rate conditions for uniform asymptotic stability of cascaded time-varying systems," *Automatica*, vol. 37, no. 3, pp. 453–460, 2001.

[39] Z. Zhang, "A flexible new technique for camera calibration," *IEEE Trans. Pattern Anal. Mach. Intell.*, vol. 22, no. 11, pp. 1330–1334, Nov. 2000.

[40] F. Yan, B. Li, W. Shi, and D. Wang, "Hybrid visual servo trajectory tracking of wheeled mobile robots," *IEEE Access*, vol. 6, pp. 24291–24298, 2018.

[41] K. Zhang, J. Chen, Y. Li, and Y. Gao, "Unified visual servoing tracking and regulation of wheeled mobile robots with an uncalibrated camera," *IEEE/ASME Trans. Mechatronics*, vol. 23, no. 4, pp. 1728–1739, Aug. 2018.

[42] F. Ke, Z. Li, H. Xiao, and X. Zhang, "Visual servoing of constrained mobile robots based on model predictive control," *IEEE Trans. Syst., Man, Cybern. Syst.*, vol. 47, no. 7, pp. 1428–1438, Jul. 2017.

[43] F. Chaumette and S. Hutchinson, "Visual servo control. I. Basic approaches," *IEEE Robot. Autom. Mag.*, vol. 13, no. 4, pp. 82–90, Dec. 2006.

[44] W. Dixon, D. Dawson, E. Zergeroglu, and A. Behal, *Nonlinear Control Wheeled Mobile Robots*. London, U.K.: Springer, 2001.

[45] B. Karan, "Calibration of kinect-type RGB-D sensors for robotic applications," *FME Trans.*, vol. 43, no. 1, pp. 47–54, 2015.

RICARDO PÉREZ-ALCOCER was born in Mérida, Mexico, in 1981. He received the B.Sc. degree in computer sciences and the M.Sc. degree in mathematics from the University of Yucatán, Mexico, in 2004 and 2007, respectively, and the Ph.D. degree in robotics and advanced manufacturing from CINVESTAV Research Center, Saltillo, Mexico, in 2013. He is currently a Research Fellow with CONACYT-Instituto Politécnico Nacional-CITEDI. His research interests include unmanned vehicles (aerial, aquatics, and wheeled), linear and nonlinear control, multiagent systems, computer vision, and intelligent systems.

LUIS GONZALO MONTOYA-VILLEGAS was born in Tijuana, Mexico, in 1992. He received the B.S. degree in electromechanical engineering from the Instituto Tecnológico de Tijuana, Tijuana, in 2015, and the M.S. degree in digital systems with specialization in control systems from CITEDI, Instituto Politécnico Nacional, Tijuana, in 2017, where he is currently pursuing the Ph.D. degree in digital systems. His research interests include the analysis and control of wheeled mobile robots, nonlinear control, multiagents systems, and consensus problems.

ANGEL EDUARDO LOPEZ-MARTINEZ was born in Puerto Vallarta, Mexico, in 1993. He received the B.E. degree in mechatronic engineering from the Universidad Tecnológica de Tijuana, Tijuana, Mexico, in 2016. He is currently pursuing the M.Sc. degree in digital systems with specialization in control systems with CITEDI, Instituto Politécnico Nacional, Tijuana. His research interests include unmanned ground vehicles, autonomous navigation, and nonlinear control.

JAVIER MORENO-VALENZUELA (Member, IEEE) received the Ph.D. degree in automatic control from CICESE Research Center, Ensenada, Mexico, in 2002. From 2004 to 2005, he was a Postdoctoral Fellow with the Université de Liége, Belgium. He is currently with CITEDI, Instituto Politécnico Nacional, Tijuana, Mexico. He is the author of many peer-reviewed journal and international conference papers. He has authored the book entitled: *Motion Control of Underactuated Mechanical Systems* (Springer-Verlag, 2018). His research interests include nonlinear systems, mechatronics, and intelligent systems. He has served as a reviewer for a number of prestigious scientific journals. He is currently an Associate Editor of the IEEE Latin America Transactions and *Mathematical Problems in Engineering*.